ChemPhysChem

Research Article
doi.org/10.1002/cphc.202200199

Chemistry Europe
European Chemical Societies Publishing

www.chemphyschem.org

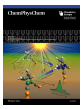

Surface Chemistry of the Molecular Solar Thermal Energy Storage System 2,3-Dicyano-Norbornadiene/Quadricyclane on Ni(111)

Felix Hemauer,[a] Udo Bauer,[a] Lukas Fromm,[b] Cornelius Weiß,[c] Andreas Leng,[c] Philipp Bachmann,[a] Fabian Düll,[a] Johann Steinhauer,[a] Valentin Schwaab,[a] Robert Grzonka,[a] Andreas Hirsch,[c] Andreas Görling,[b, d] Hans-Peter Steinrück,[a, d] and Christian Papp*[a, d, e]

Molecular solar thermal (MOST) systems are a promising approach for the introduction of sustainable energy storage solutions. We investigated the feasibility of the dicyano-substituted norbornadiene/quadricyclane molecule pair on Ni-(111) for catalytic model studies. This derivatization is known to lead to a desired bathochromic shift of the absorption maximum of the parent compound. In our experiments further favorable properties were found: At low temperatures, both molecules adsorb intact without any dissociation. *In situ* temperature-programmed HR-XPS experiments reveal the conversion of $(CN)_2$-quadricyclane to $(CN)_2$-norbornadiene under energy release between 175 and 260 K. The absence of other surface species due to side reactions indicates full isomerization. Further heating leads to the decomposition of the molecular framework into smaller carbonaceous fragments above 290 K and finally to amorphous structures, carbide and nitride above 400 K. DFT calculations gave insights into the adsorption geometries. $(CN)_2$-norbornadiene is expected to interact stronger with the surface, with flat configurations being favorable. $(CN)_2$-quadricyclane exhibits smaller adsorption energies with negligible differences for flat and side-on geometries. Simulated XP spectra are in good agreement with experimental findings further supporting the specific spectroscopic fingerprints for both valence isomers.

Introduction

With dwindling fossil fuels,[1] proceeding global warming,[2] and associated growing awareness for environmental issues, the need for green energy sources has never been higher. In addition, the worldwide energy demand is expected to exceed 27.6 TW in 2050 being more than twice the amount of 2001.[3] In this picture, solar power appears as a promising candidate for clean energy production. However, due to its intermittent character and climatic dependency, strong mismatches between load and supply arise temporally and geographically. This leads to the necessity for not only sustainable energy sources but also the development of novel energy storage technologies, ideally directly combined with the light-harvesting process.

Next to photovoltaic and electrochemical approaches, it is also possible to capture and store solar energy in a chemical manner. So-called molecular solar thermal (MOST) energy systems employ the photoconversion of an energy-lean parent molecule to an energy-rich compound in a metastable state.[4] In a reversible isomerization, the energy is stored through a rearrangement of chemical bonds and the thereby introduced strain. On demand, the backward reaction can be triggered in a catalytic or thermal way leading to the release of the stored energy. For reasonable applicability, numerous requirements have to be fulfilled: The quantum yield of the energy storage steps should be as high as possible with an absorption maximum in the range of visible light; moreover, the photoisomer must not be converted back by irradiation. Long storage times are desirable as well as high gravimetric energy densities; the latter are ensured by a low molecular weight in combination with a strong endothermic reaction profile.

Reported examples for MOST systems include stilbenes,[5] azobenzenes,[6] anthracenes,[7] or fulvalene-tetracarbonyl-

[a] F. Hemauer, Dr. U. Bauer, Dr. P. Bachmann, Dr. F. Düll, J. Steinhauer, V. Schwaab, R. Grzonka, Prof. Dr. H.-P. Steinrück, Dr. C. Papp
Lehrstuhl für Physikalische Chemie II,
Friedrich-Alexander-Universität Erlangen-Nürnberg
Egerlandstr. 3, 91058 Erlangen, Germany
[b] Dr. L. Fromm, Prof. Dr. A. Görling
Lehrstuhl für Theoretische Chemie,
Friedrich-Alexander-Universität Erlangen-Nürnberg
Egerlandstr. 3, 91058 Erlangen, Germany
[c] C. Weiß, A. Leng, Prof. Dr. A. Hirsch
Lehrstuhl für Organische Chemie II,
Friedrich-Alexander-Universität Erlangen-Nürnberg
Nikolaus-Fiebiger-Str. 10, 91058 Erlangen, Germany
[d] Prof. Dr. A. Görling, Prof. Dr. H.-P. Steinrück, Dr. C. Papp
Erlangen Catalysis Resource Center (ECRC),
Friedrich-Alexander-Universität Erlangen-Nürnberg
Egerlandstr. 3, 91058 Erlangen, Germany
[e] Dr. C. Papp
Physikalische und Theoretische Chemie, Freie Universität Berlin
Arnimallee 22, 14195 Berlin, Germany
E-mail: christian.papp@fau.de

Supporting information for this article is available on the WWW under https://doi.org/10.1002/cphc.202200199

diruthenium.[8] Another interesting system is the valence pair norbornadiene (NBD) and quadricyclane (QC), which exhibits promising properties: a comparably high reaction enthalpy (89 kJ mol^{-1})[9] and gravimetric storage density (0.97 MJ kg^{-1}), sufficient quantum yields when using photosensitizers (highest for acetophenone)[10] and a high long-term stability of the photoisomer (half-life > 14 h at 140 °C).[11] Additionally, NBD is commercially available and its isomerization has already been studied for over 50 years. Both compounds are liquids under ambient conditions enabling the usage of current transportation infrastructure. In contrast to most previous literature about reactivity in solution, heterogeneous catalysis pathways are preferred for large-scale applications. Thus, surface science investigations can deliver important insights into occurring reaction steps and conditions for decomposition and/or desorption on a heterogeneous catalyst. Especially, the mechanism of energy release and stability boundaries are of interest, as this is expected to be the bottleneck of the reaction cycle. Our fundamental study allows to assess the viability of new MOST systems in heterogeneous catalytic approaches that are necessary for application in large scale.

Earlier experiments of NBD/QC by our group on Pt(111)[12] stated a too high reactivity of the platinum surface for the cycloreversion, as QC reacts back to NBD at temperatures below 125 K. The subsequent decomposition at higher temperature proceeds over a norbornadienyl species being deprotonated at the methylene bridge. In contrast, on Ni(111)[13] both compounds are stable at 130 K, whereby the conversion of QC to NBD was found to set in at about 168 K. Thereby, benzene and methylidyne were identified as intermediate surface species upon heating. Beside the use of different surfaces/catalyst materials, the isomeric pair itself can be tailored by derivatization with functional moieties. The molecular design influences the stored heat and most importantly alters the absorption maximum, which, as mentioned, should lie in the range of visible light. Since solar energy reaching earth is peaking at ~550 nm, and the absorption onset of NBD is located at ~267 nm,[14] the introduction of suitable substituents (push-/pull-ligands) is necessary to achieve a desired bathochromic shift.[15] In particular, Moth-Poulsen *et al.* have surveyed the parameters of adequate NBD derivatives over the last years.[14,16] Unfortunately, attaching additional groups to the molecular framework increases the molecular weight and reduces the storage density. Therefore, substitution with small groups is preferred in order to maintain a high storage capacity of the system. Recently, we investigated the reaction behavior of 2,3-dibromo-norbornadiene and its valence isomer on Ni(111).[17] At ~120 K, partial dissociation of both molecules takes place. While the conversion of the quadricyclane species was observed at 170 K, the decomposition onset of $(Br)_2$-NBD was found at 190 K, with the evolution of benzene and methylidyne, analogously to unsubstituted NBD.

Herein, the results of 2,3-dicyano-substituted norbornadiene/quadricyclane on Ni(111) as a model system are discussed (see Figure 1). With a reasonable size and a red-shifted absorption onset of at least ~40 nm in comparison to parent NDB,[18] the adsorption and thermal evolution of $(CN)_2$-NBD and $(CN)_2$-QC was investigated with temperature-programmed X-ray photoelectron spectroscopy (TPXPS) allowing for *in situ* observation of surface reactions. DFT calculations were performed to investigate the adsorption properties and core level shifts of different possible adsorption geometries. The results on adsorption, triggered isomerization and decomposition are addressed.

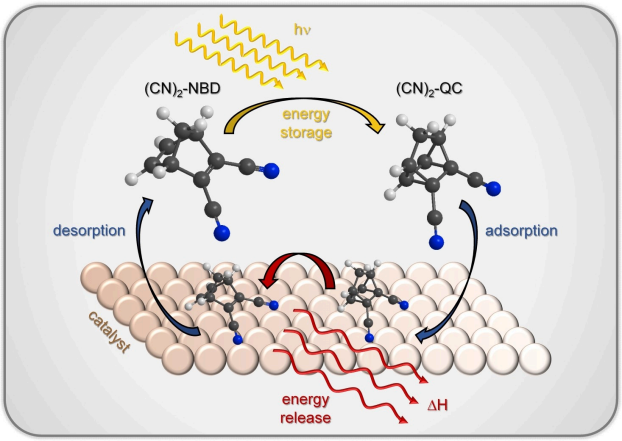

Figure 1. Schematic representation of the reversible energy storage cycle of a molecular solar thermal (MOST) system: energy storage via irradiative isomerization of $(CN)_2$-NBD to $(CN)_2$-QC, which on demand releases heat catalytically in a heterogeneous surface reaction.

Experimental Section

UHV Experiments

All discussed HR-XPS data was acquired at the synchrotron facility BESSY II of Helmholtz-Zentrum Berlin, at beamline UE56/2-PGM2. The experiments were conducted in a transportable ultra-high vacuum (UHV) apparatus comprising two main chambers, described elsewhere in detail.[19] The preparation chamber is equipped with typical tools for surface cleaning and characterization including a sputter gun, low-energy electron diffraction (LEED) optics and a multi-capillary array dosing system. In the analysis chamber, a quadrupole mass spectrometer (QMS), a three-stage supersonic molecular beam and a hemispherical electron analyzer (Omicron EA 125U7 HR) are attached. The measurements were performed in normal emission with a light incidence angle of 50°, using a photon energy of 380 eV for the C 1s region and 500 eV for the N 1s region, leading to an overall energy resolution of 180 and 220 meV, respectively.

Prior to each experiment, the cleanness of the Ni(111) single crystal (MaTeck, 99.99%) was checked by XPS. Surface contaminations were removed by ion bombardment (Ar^+, E = 1.0 keV, I_s ~ 3 μA) and subsequent annealing to 1200 K. Carbon residues were removed by O_2 dosage at 800 K. Temperatures up to 1400 K are possible by resistive heating with direct current, whereas temperatures of 130 K were achieved with liquid nitrogen cooling. A bifilar coiled filament behind the crystal allows for temperature-programmed experiments[20] with a linear heating ramp (β = 0.5 K/s) up to 550 K. Both compounds, $(CN)_2$-NBD and $(CN)_2$-QC, purified with freeze-

pump-thaw cycles, were adsorbed on the surface through the vapor pressure of the organic substances; the exposure is given in Langmuir (1 L = 10^{-6} Torr×s). The XP spectra were continuously recorded with a typical time of about 10-15 s for each spectrum during adsorption and heating. In order to avoid reactions or decomposition induced by X-ray irradiation (see Figure S6), the sample was shifted to a new position after each acquired spectrum. For data evaluation, the Fermi level was used as reference for all binding energies. The quantitative analysis is done by fitting of the signals: After subtraction of a linear background, contributions in the C 1s and N 1s spectra were fitted with peaks, described by Doniach-Šunjić functions[21] convoluted with Gaussian profiles. The coverage was determined by comparison to layers with known coverage; one monolayer (ML) corresponds to one atom per surface atom. Carbon coverages were calibrated with respect to a graphene layer,[22] which contains two carbon atoms per nickel atom (2 ML); the amount of nitrogen on the surface is equivalent to 2/9 of the carbon coverage, according to the stoichiometric ratio within the molecules.

Molecule Synthesis

2,3DibromoNorbornadiene

In a flamedried SCHLENK flask, norbornadiene (15.0 g; 163 mmol) and potassium *t*butoxide (9.43 g; 84.0 mmol) were dissolved in 100 ml of dry and degassed THF under nitrogen atmosphere. The dispersion was cooled to −78 °C and *n*butyl lithium (2.5 M in hexane; 33.2 ml; 83.0 mmol) was added dropwise over a period of 1.5 h. The mixture was warmed to −40 °C and stirred for 30 min. Afterwards it was cooled again to −78 °C and 1,2dibromoethane (3.62 ml; 42.0 mmol) was slowly added via a syringe. Once the addition was completed, the solution was warmed to −40 °C and stirred for 1 h. Before the remaining 1,2dibromoethane (10.9 ml; 126 mmol) was slowly added, the mixture was cooled again to −78 °C. The combined reagents were then stirred for 2 h at −40 °C and for additional 2 h at room temperature. The reaction was quenched by adding 100 ml of saturated $NH_4Cl_{(aq)}$ and extracted with MTBE (4×100 ml). The combined organic phases were sequentially washed with water (100 ml) and brine (100 ml) and dried over $MgSO_4$. After the solvent was removed under reduced pressure, the crude was distilled (1st fraction: 60 °C, 12 mbar, 1,2dibromoethane; 2nd fraction: 65 °C, 8 mbar, 2bromonorbornadiene; 3rd fraction: 80 °C–100 °C, 6 mbar, 2,3-dibromonorbornadiene) to give the product as a colorless oil (6.73 g; 26.9 mmol; yield = 34 %).

^{1}H-NMR ($CDCl_3$, 400 MHz): δ = 6.89 (t, J = 2 Hz, 2 H); 3.62 (t, J = 2 Hz, 2 H); 2.45 (dt, J = 6.4 Hz, 1 H); 2.18 (dt, J = 6.0 Hz, 1 H) ppm.

^{13}C-NMR ($CDCl_3$, 100 MHz): δ = 141.3; 133.1; 72.0; 58.6 ppm.

HRMS (APPI): calc. for $C_7H_6Br_2$ [M]: *m/z* = 247.8836; exp. 247.8835.

2,3DicyanoNorbornadiene

In a flamedried SCHLENK flask, 2,3dibromonorbornadiene (2.00 g; 8.00 mmol) was dissolved in 20 ml of dry DMF under a nitrogen atmosphere. After the addition of CuCN (680 mg; 7.59 mmol), the dispersion was heated to 120 °C and stirred for 2.5 h. Once the solution cooled to room temperature it was diluted with water and extracted with EtOAc (4×100 ml). Due to the formation of a black slurry, the separation of the phases is highly time consuming but can be facilitated by the addition of aqueous ammonia. The combined organic phases were sequentially washed with large amounts of water and brine and then dried over $MgSO_4$. After removing the solvent under reduced pressure, the crude was received as a yellowish oil, which was purified by column chromatography (SiO_2; hexane : DCM/1 : 4 R_f = 0.60). 2,3-Dicyanonorbornadiene was isolated as a colorless oil (275 mg; 1.93 mmol; yield = 24 %).

^{1}H-NMR ($CDCl_3$, 300 MHz): δ = 6.92 (t, J = 1.8 Hz, 2 H); 4.03 (quint, J = 2.1 Hz, 2 H); 2.40 (dt, J = 7.5 Hz, 1.5 Hz; 1 H); 2.33 (dt, J = 7.5 Hz, 1.5 Hz, 1 H) ppm [see Figure S7].

^{13}C-NMR ($CDCl_3$, 100 MHz): δ = 141.6; 141.3; 113.1; 74.9; 55.5 ppm [see Figure S8].

MS (ESI): calc. for $C_9H_6N_2$ [M + H^+]: *m/z* = 143.0609; exp. 143.1069.

2,3DicyanoQuadricyclane

2,3Dicyanonorbornadiene (100 mg; 0.703 mmol) was dissolved in 200 ml of pump-freezed methanol and irradiated for 3 h with a mercury vapor lamp. Once the solvent was removed under reduced pressure, the remaining yellow oil was purified by column chromatography (SiO_2; hexane : DCM/1 : 4 R_f = 0.27). The product was isolated as a white solid (71 mg; 0.499 mmol; yield = 71 %).

^{1}H-NMR ($CDCl_3$, 300 MHz): δ = 2.71–2.68 (m, 2 H); 2.50 (dt, J = 12.8 Hz, 1.4 Hz; 1 H); 2.41–2.38 (m, 2 H); 2.30 (dt, J = 12.4 Hz, 1.4 Hz; 1 H) ppm [see Figure S9].

^{13}C-NMR ($CDCl_3$, 100 MHz): δ = 116.1; 32.7; 32.2; 25.7; 12.8 ppm [see Figure S10].

DFT Calculations

All ab initio calculations were performed with the Vienna Ab initio Simulation Package (VASP) Version 5.4.1,[23] employing the projector-augmented wave method (PAW)[24] with a plane wave basis cutoff of 450 eV. The Perdew-Burke-Ernzerhof exchange correlation functional was used[25] together with a Methfessel-Paxton[26] smearing with a broadening width of 0.2 eV. To account for long-range intermolecular interactions, the zero damping DFT-D3 dispersion force correction scheme by Grimme was utilized.[27] The systems were calculated within a supercell approach where slabs of six Ni layers are separated by a 20 Å vacuum layer. Three of the atomic layers were fully relaxed while the other three were kept fixed to the bulk geometry with a lattice constant of 3.51 Å. To allow for non-interacting adsorbates, a 4 by 4 orthogonal unit cell was chosen to represent the surface. Brillouin zone integration was sampled with a 4×4×1 Monkhorst-Pack grid.[28] Geometries were optimized until all forces were smaller than 0.01 eV/Å. Adsorption energies were calculated as total energy differences with $E_{Ads} = E_{gas} + E_{surf} - E_{sys}$ with the total energy of the molecule in the gas phase E_{gas}, of the clean metal surface E_{surf}, and the adsorbate system E_{sys} leading to higher adsorption energies for more stable geometries. XP spectra were modeled by calculations of relative core level shifts with the method of Slater's transition state,[29] which includes final state effects (ICORELEVEL = 2, CLZ = 0.5)[30] exciting half an electron into the vacuum.

Results and Discussion

The adsorption and thermal evolution of $(CN)_2$-NBD and $(CN)_2$-QC on Ni(111) was followed *in situ* by measuring XP spectra of the C 1s and N 1s regions. In the following, the data for the two core levels are discussed separately in two sections. For easier monitoring of the conversion and surface reactions, we

concentrate on submonolayer coverages. At this coverage, information on adsorption geometries is better accessible, especially by comparison with performed DFT calculations. Complementary results with multilayer exposures are found in the supporting information.

XP Spectra of the C 1s Region

First, the adsorption of $(CN)_2$-NBD at 130 K is discussed. The C 1s spectra recorded during the adsorption experiments of $(CN)_2$-NBD are depicted as waterfall plots in Figure 2a.

The exposure of 0.24 L led to a total carbon coverage of 0.26 ML. Starting from zero coverage (Figure 2a, black bold spectrum), a characteristic line shape of the XP spectra evolves upon dosing, which can be reproduced by four peaks with constant binding energies at 285.2, 284.6, 283.6 and 283.2 eV (Figure 2c, green). While the corresponding spectral shape represents the unique spectroscopic fingerprint of the molecule, it is difficult to assign contributions to individual carbon atoms, due to the complexity of the adsorbed species and the likely coexistence of different adsorption geometries. Interestingly, the obtained spectral shape differs considerably from that of the parent molecule NBD,[13] (see Figure S4a and S4d) as $(CN)_2$-NBD features contributions at lower as well as higher binding energies. These differences are attributed to the change in the molecular structure and various adsorption geometries originating from the functionalization of the NBD framework. They also indicate that adsorption occurs in a non-dissociative manner; this suggestion is confirmed by DFT calculations of the intact molecule (see below), as the expected line shape resembles the experimental data. In addition, information of the complementary N 1s region, which are discussed later, shows no indication for fragmentation at adsorption temperature. Contributions by multilayer signals are excluded, since the corresponding signals at 285.5, 287.2, 285.6 and 284.7 eV are only observed for higher surface coverages (see Figure S2a).

The thermal evolution of $(CN)_2$-NBD on Ni(111) is investigated by TPXPS. Selected C 1s spectra are depicted in Figure 2b, along with color-coded fits of specific reaction intermediates in Figure 2c. The quantitative analysis of all spectra collected during the TPXPS experiment is provided in Figure 3a giving the amount and the temperature ranges of the respective surface species.

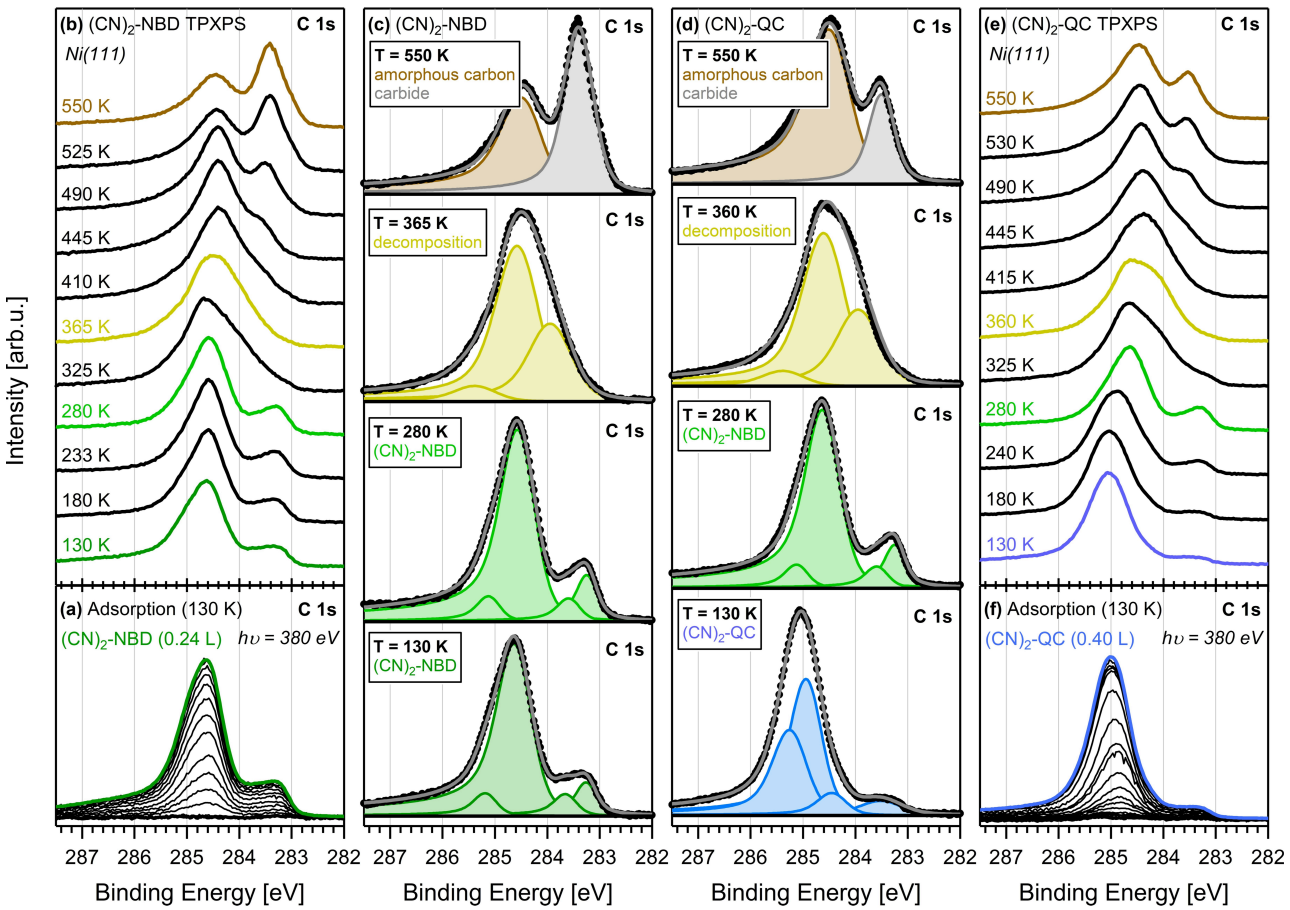

Figure 2. (a, f) Selected C 1s spectra of $(CN)_2$-NBD and $(CN)_2$-QC on Ni(111), collected during adsorption at 130 K; (b, e) subsequent TPXPS spectra (waterfall plot) during heating to 550 K; (c, d) comparison of distinct surface species for both molecules at equivalent temperatures with corresponding color-coded fits.

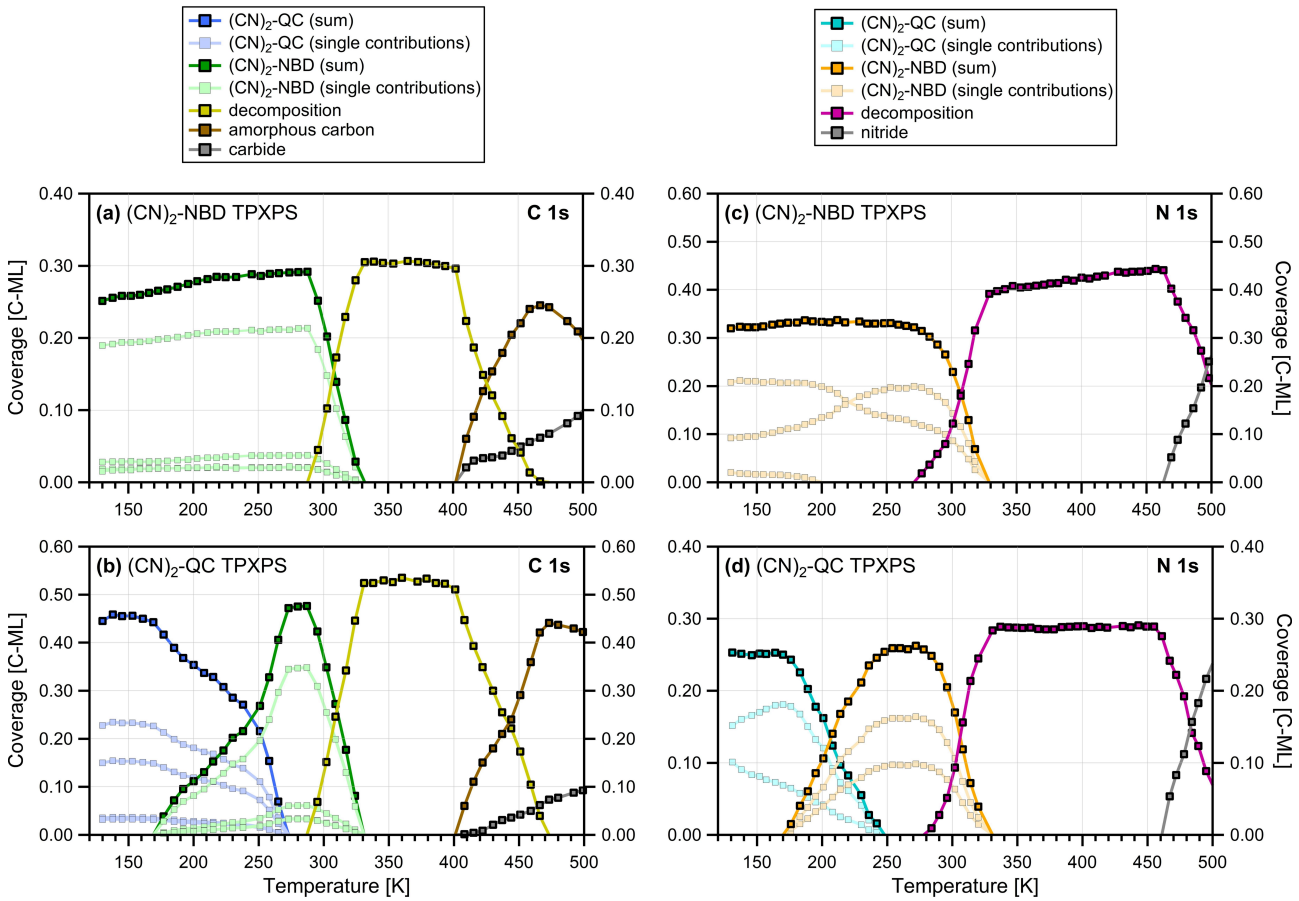

Figure 3. Quantitative analysis of the TPXP spectra of $(CN)_2$-NBD and $(CN)_2$-QC, collected with a heating rate of 0.5 K/s: (a, b) C 1s region, (c, d) N 1s region; light colors indicate contributions of single peaks to respective signal.

Below 170 K, there are only minor changes of the spectral line shape. Upon further heating to 280 K, we observe an increase of the overall carbon coverage by 16% (see Figure 3a), but no shifts of the individual peak energies (Figure 2c). Interestingly, the intensity ratio of the two higher energy peaks at 285.1 and 284.5 eV remain constant, while the two lower energy peaks at 283.6 and 283.2 eV change less than 25% in their relative intensities. From the absence of peak shifts, we conclude that no reaction has yet occurred, but instead only a rearrangement of $(CN)_2$-NBD on the surface takes place. Supplying thermal energy to the system enables mobility and facilitates transitions into thermodynamically more favored configurations. This rearrangement also explains the mentioned change in total intensity due to alterations of the attenuation behavior of the photoelectrons[31] and/or contributions by differences in photoelectron diffraction resulting from various adsorption geometries.[32]

Beginning at a temperature of ~290 K, a general broadening of the spectral line shape is observed, and the low binding energy feature characteristic of $(CN)_2$-NBD vanishes. This observation suggests the presence of a new surface species, which is fitted with three peaks at 284.5, 284.3 and 283.9 eV (Figure 2c, yellow). This species is attributed to the reaction of $(CN)_2$-NBD to carbon fragments (C_xH_y). Thermal decomposition and further dehydrogenation is common for hydrocarbons on nickel surfaces.[33] In comparison to previously investigated model systems, $(CN)_2$-NBD exhibits the highest thermal stability with the decomposition onset at 290 K: Whereas both, unsubstituted NBD[13] and $(Br)_2$-NBD,[17] react to benzene and methylidyne already at 190 and 195 K, respectively, none of these reaction products are identified for $(CN)_2$-NBD in the course of the temperature-programmed experiment here. Thus, the dicyano-substituted molecule stays intact for almost 100 K higher temperatures. Starting at ~400 K, subsequent decomposition steps take place leading to amorphous carbon,[34] yielding a peak at 284.4 eV, and carbide,[22a,35] giving a signal at 283.4 eV (Figure 2c, brown and gray).

Next, we address the adsorption and thermal evolution of $(CN)_2$-QC on Ni(111). The adsorption of $(CN)_2$-QC at 130 K up to an exposure of 0.40 L was followed by XPS (Figure 2f), yielding a carbon coverage of 0.40 ML. The characteristic line shape of the XP spectra is fitted with four peaks at binding energies of 285.2, 284.9, 284.4 and 283.5 eV (Figure 2d, blue). Again, no assignment to distinct carbon atoms is given due to the complexity of the adsorption system, but the peaks can serve as a spectral fingerprint. As in the case of $(CN)_2$-NBD, the

comparison of $(CN)_2$-QC with unsubstituted QC[13] reveals a deviating line shape (see Figure S5a and S5d): While $(CN)_2$-QC displays major contributions above 285 eV, pure QC has a distinct peak at 283.4 eV. When comparing the two dicyano-substituted molecules, that is, $(CN)_2$-NBD and $(CN)_2$-QC, we observe very different spectra: Not only the binding energies of the four peaks used for fitting do not match, but also their relative intensities differ strongly. The differences between the spectra of $(CN)_2$-QC to those of unsubstituted QC and $(CN)_2$-NBD suggest a non-dissociative adsorption without conversion at low temperatures; this presumption is verified in the following discussion of the observed quantitative back reaction of $(CN)_2$-QC to $(CN)_2$-NBD. We can also rule out contributions from $(CN)_2$-QC multilayers, which would show three peaks at 287.4, 286.2, and 284.8 eV (see Figure S2f).

The thermal evolution of the valence isomer $(CN)_2$-QC is shown in Figure 2e, along with the quantitative analysis in Figure 3b. For the peak fitting, the intensity ratios of the fitted peaks at 285.2, 284.9, 284.4 and 283.5 eV were kept fixed. Up to 175 K, no changes of the binding energy positions are observed. At higher temperatures, changes of the spectral fingerprint become visible, indicative of the onset of the conversion of $(CN)_2$-QC to $(CN)_2$-NBD. The peaks related to $(CN)_2$-QC drop in intensity and have completely vanished at ~270 K; simultaneously, $(CN)_2$-NBD has become the solely detected species. The comparison of the fitted C 1s TPXP spectra of $(CN)_2$-NBD in Figure 2c and $(CN)_2$-QC in Figure 2d confirms the isomerization of $(CN)_2$-QC to $(CN)_2$-NBD: At 280 K, the spectra from both TPXPS series (Figure 2c and 2d, green) are fitted with the same parameters; their identical appearance proves the presence of an equivalent surface species; the only minor difference is a shift of the main peak by less than 0.1 eV to higher binding energy for $(CN)_2$-QC, which is within the accuracy of measurement and evaluation. The formed $(CN)_2$-NBD has a maximum coverage of 0.48 ML at 270 K. The absence of other surface species indicates full conversion. Although the temperature range from 175 to 260 K for the isomerization of $(CN)_2$-QC to $(CN)_2$-NBD is rather large (see Figure 3b), the relatively high onset for the reaction is of advantage for applications towards ambient conditions. The further thermal evolution is expected to be analogous to the $(CN)_2$-NBD experiment. Indeed, at 290 K, identical decomposition signals are found (Figure 2d, yellow), due to dissociation into C_xH_y fragments.[33] Finally, when heating to above 400 K, amorphous carbon structures[34] and contributions by carbide[22a,35] are observed (Figure 2d, brown and gray), as in the case of $(CN)_2$-NBD.

As next step, we performed DFT calculations in order to understand the interactions of the molecular pair with the surface and to obtain insights into the spectral fingerprints. Similar to previous results of NBD adsorption on surfaces, different adsorption motifs are conceivable.[12–13] For this reason, a flat (η^2:η^2) geometry, in which NBD is bound via both its double bonds to the surface, and a side-on (η^2:η^1) geometry, in which only one double bond and the CH_2 bridgehead are bound to the surface, were regarded. In addition to these two basic motifs, different positions relative to the surface were considered. The most stable geometries are depicted in Figure 4.

As reported previously, the bond of NBD via the C=C double bond to the surface is a strong interaction leading to very stable structures. Therefore, for $(CN)_2$-NBD, a "flat-like" adsorption via both double bonds (structure 4a–4c) is preferred and yields higher adsorption energies of about 3.6 to up to 4.0 eV, compared to values ranging from 1.4 eV for geometries with CN-groups pointing away from the surface to ~2.1 eV for the side-on adsorption motif (structure 4d). Unlike in the case of the $(Br)_2$-NBD,[17] the CN-groups are not as bulky as the bromine atoms and offer more flexibility. In this way, they do not hinder the NBD moiety to interact with both C=C double bonds with the surface. Still, there are slight differences regarding the position of the molecule on the surface. In case of the "flat-like"

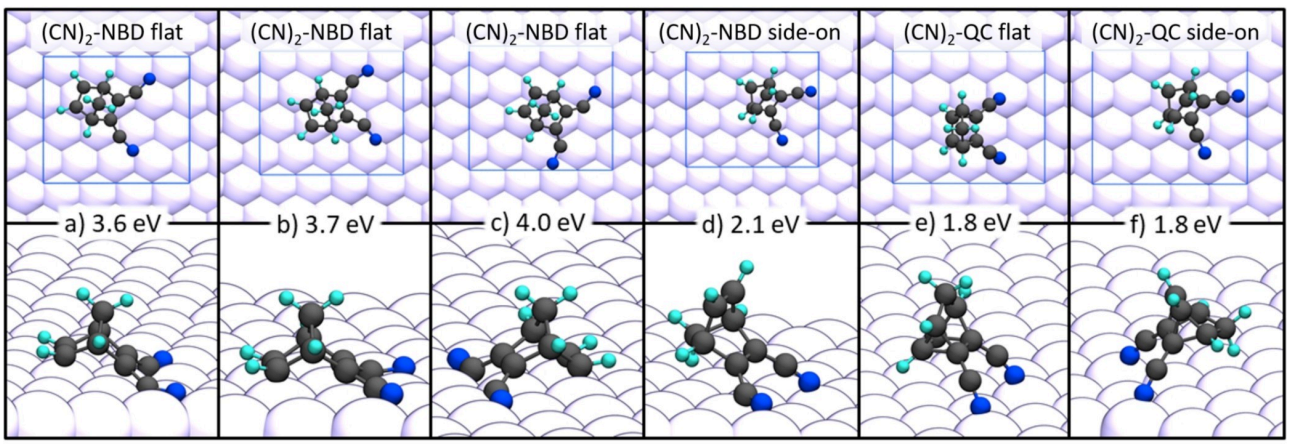

Figure 4. Adsorption geometries calculated with DFT: (a–c) different geometries for a flat adsorbed $(CN)_2$-NBD, (d) side-on adsorbed $(CN)_2$-NBD, (e) flat adsorbed $(CN)_2$-QC, (f) side-on adsorbed $(CN)_2$-QC; corresponding adsorption energies are given; carbon atoms depicted in black, hydrogen in turquoise, nitrogen in blue, nickel surface in white, unit cells are indicated by a blue rectangle.

adsorption, we observe a preference for a CN adsorption in a bridge-like adsorption (structure 4a–4c). Furthermore, the most stable structure (4c) is bound with the C=C double bond without the CN-groups to two surface atoms and additionally on the other side with the CN-groups to a single Ni atom. The CN-groups are bending outwards to occupy their preferred bridge position. This structure is with 4.0 eV about 0.3 eV more stable than the rest of the structures.

During the adsorption process at low temperature, it is very likely that the $(CN)_2$-NBD molecules stick randomly to the surface in one of the several possible geometries and stay in this way. Thus, a mixture of different structures is present. Heating the sample then provides enough energy to overcome the barrier for flipping and moving the molecules from, e.g., the less stable side-on to the more stable flat geometry, which explains the change of the spectral features in the temperature range from 130–175 K.

For $(CN)_2$-QC, the adsorption in both orientations (structure 4e and 4f) is with 1.8 eV similarly stable. Thus, we assume a mixed adsorption. Because of the other bonding situation in QC with no double bonds, the interaction with the surface is different. The molecule is rather compact and offers mainly the CN-groups to interact with the surface. Therefore, in both stable geometries the nitrogen atoms of the CN-groups are bound to surface nickel atoms in an on-top position. The difference between the two geometries (4e, 4f) is that in the "flat-like" geometry two hydrogen atoms of the strained four-membered ring are weakly interacting with the surface, whereas in the side-on geometry the CH_2 group is doing so. In both cases, this is a weak dispersion interaction, explaining the small energy differences.

Calculations of the relative core level shifts for the different geometries (see Figure 5) corroborate the presence of unreacted $(CN)_2$-QC on the surface. The spectra show higher binding energies for the QC derivative, which is also observed in the experiments. In general, a good correspondence of the calculated to the experimental spectra is found. But unfortunately, it is not possible to make a clear assignment to the structures. The shoulder at low binding energies can be assigned to the strongly interacting C=C double bond. Because of the lack of this interaction in the QC derivative, this spectral feature is not present. Additionally, this is the feature increasing in intensity during the proposed rearrangement from the side-on to the flat geometry.

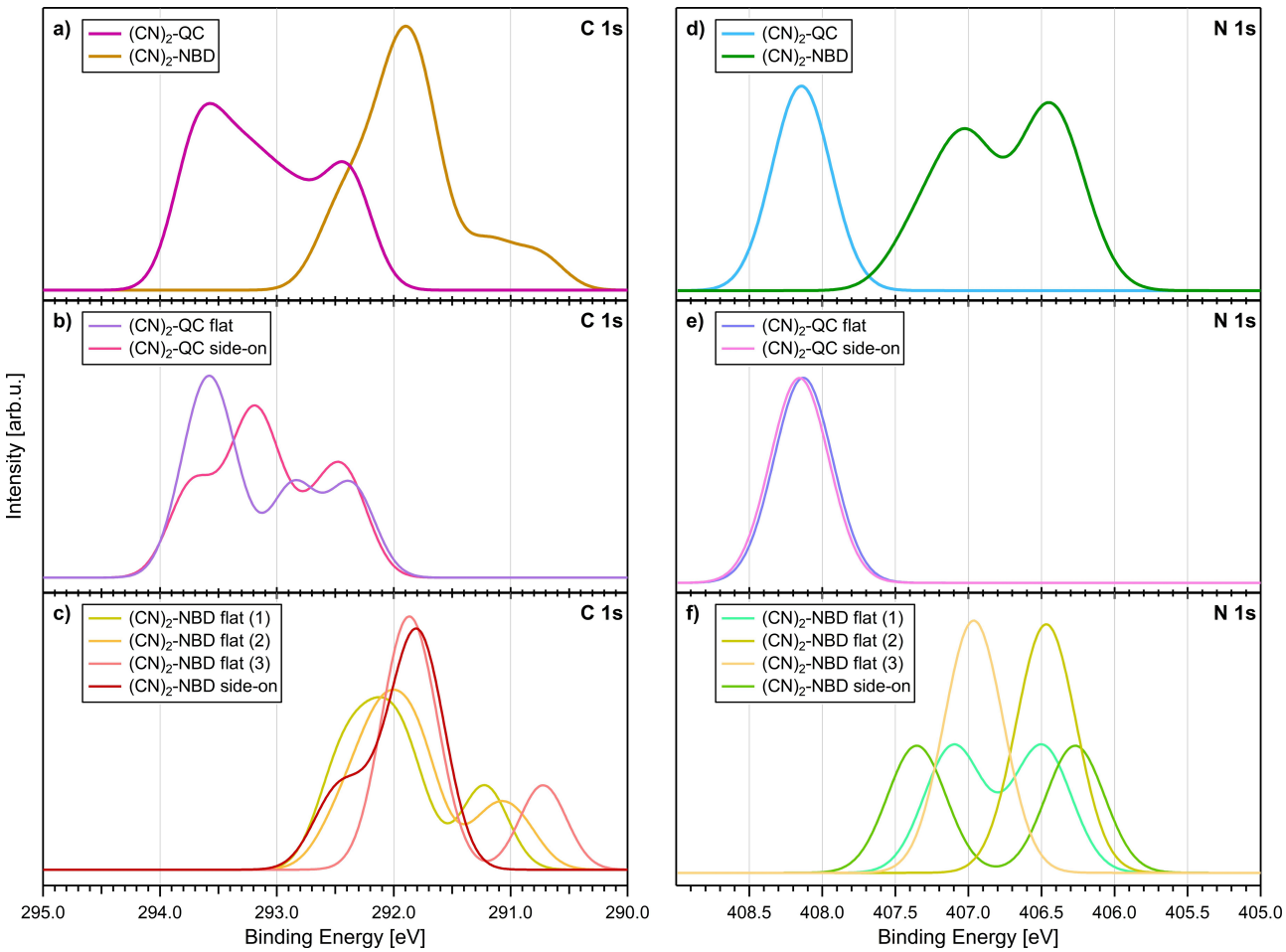

Figure 5. Representation of calculated XP spectra: (a–c) depiction of C 1s region results, whereby (a) gives a comparison of $(CN)_2$-NBD and $(CN)_2$-QC as total sum of (b, c) single contributions of different adsorption geometries; (d–f) depiction of N 1s region results of the molecule pair with (d) sum of respective signals and (e, f) spectra of single adsorption geometries; all spectra were generated by Gaussian functions with a width of 0.02 eV.

XP Spectra of the N 1s Region

Complementary information on the adsorption and thermal evolution is obtained from XP spectra of the N 1s region. The N 1s spectra acquired during exposure of the Ni(111) surface to $(CN)_2$-NBD and $(CN)_2$-QC are depicted in Figure 6a and 6f, respectively. For $(CN)_2$-NBD, an asymmetric peak evolves at 397.9 eV with a broad shoulder towards higher binding energy, yielding a total carbon coverage of 0.32 ML after a dosage of 0.34 L. In order to obtain a reasonable fit, three peaks at 399.5, 398.3 and 397.8 eV had to be used (Figure 6c, orange). This is rather surprising, since it was expected that both nitrogen atoms in the symmetric molecular framework of $(CN)_2$-NBD show an equivalent behavior, which would imply the existence of only one peak. Multilayer formation is ruled out by comparison to the spectrum of multilayers with larger exposure, which show two peaks at 400.2 and 399.1 eV (see Figure S3a). Instead, we attribute the necessity of three peaks to various adsorption sites and/or geometries. In contrast to the structurally related dibromo-substituted $(Br)_2$-NBD and $(Br)_2$-QC,[17] there are no indications that fragmentation takes place upon adsorption. Notably, the observed binding energies do not match those characteristic of atomic nitrogen (~397 eV)[36] or cyanide fragments (~397.5 eV) on nickel.[37]

Representative XP spectra of the thermal evolution are shown in Figure 6b, along with color-coded fits of specific reaction intermediates in Figure 6c. The quantitative analysis of all spectra collected during the TPXPS experiment is provided in Figure 3c. As the nitrogen atoms are part of the cyano groups attached to the NBD/QC framework, it is expected that changes of the adsorption geometries have a more pronounced effect in the N 1s than in the C 1s spectra. On the other hand, effects in the spectra of the conversion reaction are assumed to be less distinct in the N 1s region. At the start of the heating ramp, the peak at 397.8 eV exhibits the highest intensity (0.21 ML). Upon heating, the peak at 398.3 eV grows at the expense of the two other two peaks. At ~190 K, the peak at 399.5 eV has vanished, and at 230 K the peak at 398.3 eV surpasses that at 397.8 eV becoming the dominant surface species at 270 K; simultaneously, the two remaining peaks shift by 0.07 eV towards lower binding energies, while the overall coverage stays roughly constant until 270 K (see Figure 3c). The change and even inversion in relative intensities as well as the small peaks shifts are attributed to rearrangement steps occurring upon heating from low temperatures of 130 K, as also discussed for the C 1s region. The rearrangement is finished until ~270 K. (Figure 6c, light orange). Starting at ~280 K, the peak with the maximum at 398.3 eV vanishes until 330 K, and a new asymmetric peak evolves at 397.6 eV (Figure 6c, purple), which is assigned to

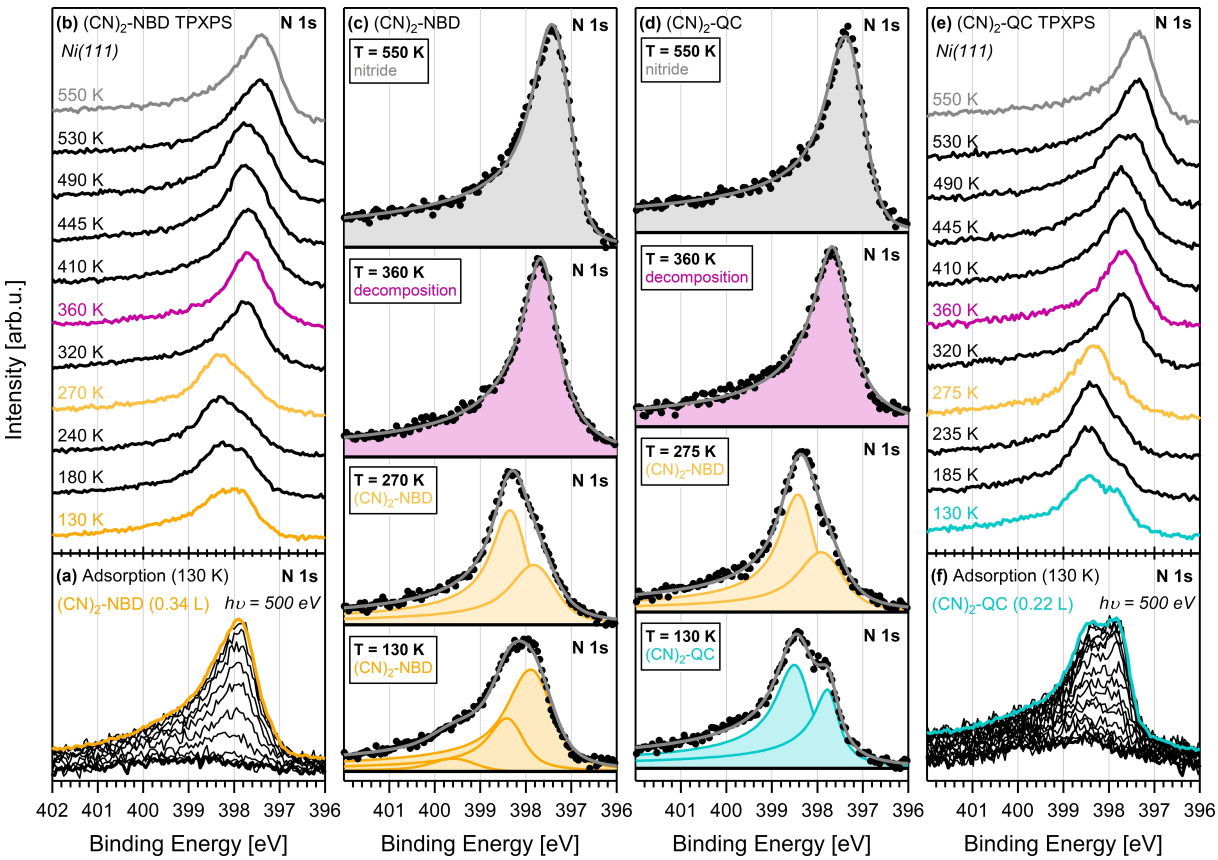

Figure 6. (a, f) Selected N 1s spectra of $(CN)_2$-NBD and $(CN)_2$-QC on Ni(111), collected during adsorption at 130 K; (b, e) subsequent TPXPS spectra (waterfall plot) during heating to 550 K; (c, d) comparison of distinct surface species for both molecules at equivalent temperatures with corresponding color-coded fits.

decomposition products. This observation is in good agreement with the temperature onset identified in the C 1s spectra. The cleavage of the carbon bond between cyano group and NBD framework results into the detachment of the cyano moieties.[37–38] This new spectral shape maintains from 330 to 460 K. The slight increase in coverage by about 10% is explained by different diffraction behavior of the formed compounds depending on their orientation on the surface.[32] Further heating gives rise to a broad, asymmetric signal developing at 470 K, which is fitted with one asymmetric peak at 397.3 eV (Figure 6c, gray). According to literature, this final signal is assigned to nitride emerging upon CN fragmentation.[33a,36]

The N 1s spectra collected during the adsorption of the valence isomer $(CN)_2$-QC are depicted in Figure 6f; the black bold spectrum at the bottom was acquired prior to exposure, while its slightly curved background indicates minor impurities on the surface. During dosing, a characteristic line shape evolves, which was fitted with two asymmetric peaks at 398.4 and 397.7 eV (Figure 6d, turquoise). For the largest exposure of 0.22 L, a carbon coverage of 0.25 ML was obtained. Analogous to $(CN)_2$-NBD, the two peaks are attributed to different adsorption sites and/or geometries on the surface. Contributions from multilayers are not found by comparison to the spectrum of multilayers with two peaks at 400.2 and 399.7 eV (see Figure S3f). Even though the peak maxima of $(CN)_2$-NBD and $(CN)_2$-QC have almost identical binding energies, the characteristic line shapes serve as fingerprint for the respective molecule. This is due to the different intensity ratios and number of the fitted peaks, which make the molecule pair clearly distinguishable also in the N 1s region.

Selected XP spectra of the TPXPS experiment of $(CN)_2$-QC are depicted in Figure 6e, along with color-coded fits in Figure 6d; the quantification is given in Figure 3d. Up to 170 K, the total coverage remains constant. The peak at 398.4 eV increases until this temperature to a maximum of 0.18 ML at the expense of the peak at 397.7 eV, which is linearly declining (see Figure 3d). The temperature of 170 K also marks the onset of the evolution of a more narrow signal, which can be fitted with exactly the same parameters as for $(CN)_2$-NBD. Hence, the conversion of $(CN)_2$-QC to $(CN)_2$-NBD is confirmed in the N 1s spectra at the same temperature as in the C 1s spectra. At 250 K, the isomerization is completed, yielding $(CN)_2$-NBD as only surface species (Figure 6d, light orange). From this temperature on, an analogous reaction pathway is observed for $(CN)_2$-QC and $(CN)_2$-NBD. Above ~280 K, the same fragmentation product is detected with a peak at 397.6 eV (Figure 6d, purple) attributed to cleaved cyano groups on the surface.[37–38] Above 470 K, the formation of nitride as final decomposition product is deduced from the asymmetric peak at 397.3 eV (Figure 6d, gray).[33a,36]

Conclusions

We investigated the surface chemistry of dicyano-norbornadiene/quadricyclane on Ni(111) with HR-XPS, supported by DFT calculations. The adsorption of $(CN)_2$-NBD and $(CN)_2$-QC yields distinguishable spectroscopic fingerprints in the C 1s and N 1s regions, which are characteristic of the respective molecule. In addition, no indications for dissociation upon adsorption are found. Results from DFT calculations show that the adsorption in flat geometries ($\eta^2:\eta^2$) is energetically favored for $(CN)_2$-NBD, whereas the weaker bound $(CN)_2$-QC displays minor energetic differences in different adsorption motifs. During adsorption at low temperature, the activation barrier to find the lowest energy is not overcome, leading to a mixture of different adsorption geometries. When supplying thermal energy to the system, we propose a rearrangement step for $(CN)_2$-NBD into its most favorable geometry. Simulated XP spectra confirm the spectroscopic differences of $(CN)_2$-NBD and $(CN)_2$-QC.

Starting at 175 K, the conversion of $(CN)_2$-QC to $(CN)_2$-NBD is spectroscopically observed, while $(CN)_2$-NBD is the solely detectable surface species at 260 K. Upon heating above 290 K, the molecular framework of $(CN)_2$-NBD decomposes with the detachment of the cyano moiety. Above 400 K, amorphous carbon structures, carbide and nitride are formed (see Scheme 1). In contrast to parent NBD and dibromo-substituted NBD on Ni(111), benzene and methylidyne as decomposition intermediates are not formed during thermal evolution. In comparison, the dicyano-substituted system seems superior with an about 100 K higher onset of decomposition.[13,17] Thus,

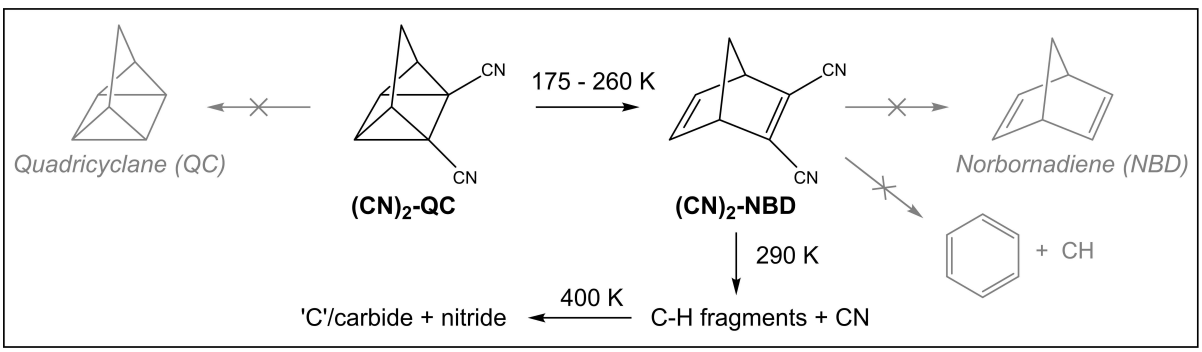

Scheme 1. Proposed reaction pathway of $(CN)_2$-QC on Ni(111): onset of cycloreversion reaction to $(CN)_2$-NBD at 175 K, being completed at 260 K; beginning decomposition into C–H fragments and CN for temperatures above 290 K; final observation of amorphous carbon, carbide and nitride species.

our study demonstrates that the reactivity of the norbornadiene/quadricyclane system can be strongly influenced by the choice of the functional group, with the cyano moieties being electronically similar to halides, but smaller and more flexible. The successful monitoring of the cyclorversion reaction and the high thermal stability gives the general practicality of the surveyed model system as promising candidate for future MOST applications.

Acknowledgements

The work was supported by the Cluster of Excellence 'Engineering of Advanced Materials' and the Deutsche Forschungsgemeinschaft (DFG) – Project No. 392607742. We thank Helmholtz-Zentrum Berlin for the allocation of synchrotron radiation beamtime and the BESSY II staff for support during beamtime. Open Access funding enabled and organized by Projekt DEAL.

Conflict of Interest

The authors declare no conflict of interest.

Data Availability Statement

The data that support the findings of this study are available from the corresponding author upon reasonable request.

Keywords: catalysis · energy storage · MOST system · photoelectron spectroscopy · surface reactions

[1] a) M. Höök, X. Tang, *Energy Policy* **2013**, *52*, 797–809; b) British Petroleum, *Statistical Review of World Energy* **2020**, 69.
[2] M. Meinshausen, N. Meinshausen, W. Hare, S. C. Raper, K. Frieler, R. Knutti, D. J. Frame, M. R. Allen, *Nature* **2009**, *458*, 1158–1162.
[3] N. S. Lewis, D. G. Nocera, *Proc. Natl. Acad. Sci. USA* **2006**, *103*, 15729–15735.
[4] a) A. Lennartson, A. Roffey, K. Moth-Poulsen, *Tetrahedron Lett.* **2015**, *56*, 1457–1465; b) K. Moth-Poulsen, D. Ćoso, K. Börjesson, N. Vinokurov, S. K. Meier, A. Majumdar, K. P. C. Vollhardt, R. A. Segalman, *Energy Environ. Sci.* **2012**, *5*; c) K. Börjesson, A. Lennartson, K. Moth-Poulsen, *ACS Sustainable Chem. Eng.* **2013**, *1*, 585–590; d) T. J. Kucharski, Y. C. Tian, S. Akbulatov, R. Boulatov, *Energy Environ. Sci.* **2011**, *4*, 4449–4472; e) C. L. Sun, C. Wang, R. Boulatov, *ChemPhotoChem* **2019**, *3*, 268–283; f) Z. Wang, A. Roffey, R. Losantos, A. Lennartson, M. Jevric, A. U. Petersen, M. Quant, A. Dreos, X. Wen, D. Sampedro, K. Börjesson, K. Moth-Poulsen, *Energy Environ. Sci.* **2019**, *12*, 187–193.
[5] a) D. Schulte-Frohlinde, H. Blume, H. Güsten, *J. Phys. Chem.* **1962**, *66*, 2486–2491; b) D. H. Waldeck, *Chem. Rev.* **1991**, *91*, 415–436; c) C. Bastianelli, V. Caia, G. Cum, R. Gallo, V. Mancini, *J. Chem. Soc. Perkin Trans. 2* **1991**, 679–683.
[6] a) H. Taoda, K. Hayakawa, K. Kawase, H. Yamakita, *J. Chem. Eng. Jpn.* **1987**, *20*, 265–270; b) H. M. Bandara, S. C. Burdette, *Chem. Soc. Rev.* **2012**, *41*, 1809–1825; c) A. M. Kolpak, J. C. Grossman, *Nano Lett.* **2011**, *11*, 3156–3162; d) K. Masutani, M. A. Morikawa, N. Kimizuka, *Chem. Commun.* **2014**, *50*, 15803–15806; e) Z. Wang, R. Losantos, D. Sampedro, M. Morikawa, K. Börjesson, N. Kimizuka, K. Moth-Poulsen, *J. Mater. Chem. A* **2019**, *7*, 15042–15047.
[7] a) G. Jones, T. E. Reinhardt, W. R. Bergmark, *Sol. Energy* **1978**, *20*, 241–248; b) J. F. Xu, Y. Z. Chen, L. Z. Wu, C. H. Tung, Q. Z. Yang, *Org. Lett.* **2013**, *15*, 6148–6151.
[8] a) K. P. C. Vollhardt, T. W. Weidman, *J. Am. Chem. Soc.* **1983**, *105*, 1676–1677; b) R. Boese, J. K. Cammack, A. J. Matzger, K. Pflug, W. B. Tolman, K. P. C. Vollhardt, T. W. Weidman, *J. Am. Chem. Soc.* **1997**, *119*, 6757–6773; c) Y. Kanai, V. Srinivasan, S. K. Meier, K. P. Vollhardt, J. C. Grossman, *Angew. Chem. Int. Ed.* **2010**, *49*, 8926–8929; *Angew. Chem.* **2010**, *122*, 9110–9113; d) K. Börjesson, D. Ćoso, V. Gray, J. C. Grossman, J. Guan, C. B. Harris, N. Hertkorn, Z. Hou, Y. Kanai, D. Lee, J. P. Lomont, A. Majumdar, S. K. Meier, K. Moth-Poulsen, R. L. Myrabo, S. C. Nguyen, R. A. Segalman, V. Srinivasan, W. B. Tolman, N. Vinokurov, K. P. Vollhardt, T. W. Weidman, *Chem. Eur. J.* **2014**, *20*, 15587–15604; e) A. Lennartson, A. Lundin, K. Börjesson, V. Gray, K. Moth-Poulsen, *Dalton Trans.* **2016**, *45*, 8740–8744.
[9] X. W. An, Y. D. Xie, *Thermochim. Acta* **1993**, *220*, 17–25.
[10] H. Taoda, K. Hayakawa, K. Kawase, *J. Chem. Eng. Jpn.* **1987**, *20*, 335–338.
[11] G. S. Hammond, N. J. Turro, A. Fischer, *J. Am. Chem. Soc.* **1961**, *83*, 4674–4675.
[12] U. Bauer, S. Mohr, T. Dopper, P. Bachmann, F. Späth, F. Düll, M. Schwarz, O. Brummel, L. Fromm, U. Pinkert, A. Gorling, A. Hirsch, J. Bachmann, H.-P. Steinrück, J. Libuda, C. Papp, *Chem. Eur. J.* **2017**, *23*, 1613–1622.
[13] U. Bauer, L. Fromm, C. Weiß, P. Bachmann, F. Späth, F. Düll, J. Steinhauer, W. Hieringer, A. Görling, A. Hirsch, H.-P. Steinrück, C. Papp, *J. Phys. Chem. C* **2018**, *123*, 7654–7664.
[14] M. Quant, A. Lennartson, A. Dreos, M. Kuisma, P. Erhart, K. Börjesson, K. Moth-Poulsen, *Chem. Eur. J.* **2016**, *22*, 13265–13274.
[15] a) V. A. Bren′, A. D. Dubonosov, V. I. Minkin, V. A. Chernoivanov, *Russ. Chem. Rev.* **1991**, *60*, 451–469; b) A. D. Dubonosov, V. A. Bren, V. A. Chernoivanov, *Russ. Chem. Rev.* **2002**, *71*, 917–927.
[16] a) V. Gray, A. Lennartson, P. Ratanalert, K. Börjesson, K. Moth-Poulsen, *Chem. Commun.* **2014**, *50*, 5330–5332; b) K. Jorner, A. Dreos, R. Emanuelsson, O. El Bakouri, I. Fdez. Galván, K. Börjesson, F. Feixas, R. Lindh, B. Zietz, K. Moth-Poulsen, H. Ottosson, *J. Mater. Chem. A* **2017**, *5*, 12369–12378; c) A. Dreos, Z. Wang, J. Udmark, A. Ström, P. Erhart, K. Börjesson, M. B. Nielsen, K. Moth-Poulsen, *Adv. Energy Mater.* **2018**, *8*; d) M. Jevric, A. U. Petersen, M. Mansø, S. Kumar Singh, Z. Wang, A. Dreos, C. Sumby, M. B. Nielsen, K. Börjesson, P. Erhart, K. Moth-Poulsen, *Chem. Eur. J.* **2018**, *24*, 12767–12772; e) M. Mansø, A. U. Petersen, Z. Wang, P. Erhart, M. B. Nielsen, K. Moth-Poulsen, *Nat. Commun.* **2018**, *9*, 1945; f) M. Mansø, B. E. Tebikachew, K. Moth-Poulsen, M. B. Nielsen, *Org. Biomol. Chem.* **2018**, *16*, 5585–5590; g) M. D. Kilde, M. Mansø, N. Ree, A. U. Petersen, K. Moth-Poulsen, K. V. Mikkelsen, M. B. Nielsen, *Org. Biomol. Chem.* **2019**, *17*, 7735–7746; h) M. Mansø, L. Fernandez, Z. Wang, K. Moth-Poulsen, M. B. Nielsen, *Molecules* **2020**, *25*; i) J. Orrego-Hernández, A. Dreos, K. Moth-Poulsen, *Acc. Chem. Res.* **2020**, *53*, 1478–1487.
[17] U. Bauer, L. Fromm, C. Weiss, F. Späth, P. Bachmann, F. Düll, J. Steinhauer, S. Matysik, A. Pominov, A. Gorling, A. Hirsch, H.-P. Steinrück, C. Papp, *J. Chem. Phys.* **2019**, *150*, 184706.
[18] a) Y. Harel, A. W. Adamson, C. Kutal, P. A. Grutsch, K. Yasufuku, *J. Phys. Chem.* **1987**, *91*, 901–904; b) W. L. Dilling, *Chem. Rev.* **1966**, *66*, 373–393; c) Z.-i. Yoshida, *J. Photochem.* **1985**, *29*, 27–40.
[19] R. Denecke, M. Kinne, C. M. Whelan, H.-P. Steinrück, *Surf. Rev. Lett.* **2002**, *09*, 797–801.
[20] a) C. Papp, H.-P. Steinrück, *Surf. Sci. Rep.* **2013**, *68*, 446–487; b) A. Baraldi, G. Comelli, S. Lizzit, D. Cocco, G. Paolucci, R. Rosei, *Surf. Sci.* **1996**, *367*, L67-L72.
[21] S. Doniach, M. Sunjic, *J. Phys. C* **1970**, *3*, 285–291.
[22] a) W. Zhao, S. M. Kozlov, O. Höfert, K. Gotterbarm, M. P. A. Lorenz, F. Viñes, C. Papp, A. Görling, H.-P. Steinrück, *J. Phys. Chem. Lett.* **2011**, *2*, 759–764; b) R. Addou, A. Dahal, P. Sutter, M. Batzill, *Appl. Phys. Lett.* **2012**, *100*, 021601.
[23] a) G. Kresse, J. Hafner, *Phys. Rev. B* **1993**, *47*, 558–561; b) G. Kresse, J. Furthmüller, *Comput. Mater. Sci.* **1996**, *6*, 15–50; c) G. Kresse, J. Furthmüller, *Phys. Rev. B* **1996**, *54*, 11169–11186.
[24] G. Kresse, D. Joubert, *Phys. Rev. B* **1999**, *59*, 1758–1775.
[25] J. P. Perdew, K. Burke, M. Ernzerhof, *Phys. Rev. Lett.* **1996**, *77*, 3865–3868.
[26] M. Methfessel, A. T. Paxton, *Phys. Rev. B* **1989**, *40*, 3616–3621.
[27] S. Grimme, J. Antony, S. Ehrlich, H. Krieg, *J. Chem. Phys.* **2010**, *132*, 154104.
[28] H. J. Monkhorst, J. D. Pack, *Phys. Rev. B* **1976**, *13*, 5188–5192.
[29] a) J. C. Slater, in *Advances in Quantum Chemistry, Vol. 6* (Ed.: P.-O. Löwdin), Academic Press, **1972**, pp. 1–92; b) J. F. Janak, *Phys. Rev. B* **1978**, *18*, 7165–7168.
[30] L. Köhler, G. Kresse, *Phys. Rev. B* **2004**, *70*.
[31] C. J. Powell, A. Jablonski, *Nucl. Instrum. Methods Phys. Res. Sect. A* **2009**, *601*, 54–65.

[32] D. P. Woodruff, A. M. Bradshaw, *Rep. Prog. Phys.* **1994**, *57*, 1029–1080.
[33] a) I. Chorkendorff, J. N. Russell, J. T. Yates, *J. Chem. Phys.* **1987**, *86*, 4692–4700; b) S. X. Huang, D. A. Fischer, J. L. Gland, *J. Phys. Chem.* **1996**, *100*, 13629–13635; c) S. Lehwald, H. Ibach, *Surf. Sci.* **1979**, *89*, 425–445; d) C. Papp, R. Denecke, H.-P. Steinrück, *Langmuir* **2007**, *23*, 5541–5547.
[34] a) R. Haerle, E. Riedo, A. Pasquarello, A. Baldereschi, *Phys. Rev. B* **2001**, *65*, 045101; b) J. Diaz, G. Paolicelli, S. Ferrer, F. Comin, *Phys. Rev. B* **1996**, *54*, 8064–8069; c) P. K. Chu, L. Li, *Mater. Chem. Phys.* **2006**, *96*, 253–277; d) C. Ronning, H. Feldermann, R. Merk, H. Hofsäss, P. Reinke, J. U. Thiele, *Phys. Rev. B* **1998**, *58*, 2207–2215.
[35] a) A. Wiltner, C. Linsmeier, *Phys. Status Solidi* **2004**, *201*, 881–887; b) M. Wei, Q. Fu, Y. Yang, W. Wei, E. Crumlin, H. Bluhm, X. H. Bao, *J. Phys. Chem. C* **2015**, *119*, 13590–13597.
[36] a) M. J. Grunze, J. Fühler, M. Neumann, C. R. Brundle, D. J. Auerbach, J. Behm, *Surf. Sci.* **1984**, *139*, 109–120; b) C. N. R. Rao, G. Ranga Rao, *Surf. Sci. Rep.* **1991**, *13*, 223–263; c) W. F. Egelhoff, *Phys. Rev. B* **1984**, *29*, 3681–3683.
[37] a) R. Gouttebaron, S. Bourgeois, M. Perdereau, *Surf. Sci.* **2000**, *458*, 239–246; b) T. Nakayama, K. Inamura, Y. Inoue, S. Ikeda, K. Kishi, *Surf. Sci.* **1987**, *179*, 47–58.
[38] a) K. Kishi, Y. Ehara, *Surf. Sci.* **1986**, *176*, 567–577; b) J. C. Hemminger, E. L. Muetterties, G. A. Somorjai, *J. Am. Chem. Soc.* **1979**, *101*, 62–67.

Manuscript received: March 24, 2022
Revised manuscript received: May 23, 2022
Accepted manuscript online: May 25, 2022
Version of record online: June 29, 2022